Zero-dimensional chemical kinetic simulation of ROS/RNSin pulsed pulsed-discharge exposed water

Zero-dimensional chemical kinetic simulation of ROS/RNS in pulsed-discharge exposed water

Kazuhiro Takahashi[1,*], Satoru Kawaguchi[1,2], Kohki Satoh[1], Hideki Kawaguchi[1], Igor Timoshkin[3], Martin Given[3], and Scott MacGregor[3]

[1]*Muroran Institute of Technology, Muroran, Hokkaido 050-8585, Japan*

[2]*Research fellow of Japan Society for the Promotion of Science*

[3]*University of Strathclyde, Glasgow G1 1XW, U.K.*

[*]E-mail: ktakahashi@mmm.muroran-it.ac.jp

The concentration variations of reactive oxygen/nitrogen species in water, such as H_2O_2, NO_2^-, and NO_3^- generated by pulsed-discharge plasma exposure, are calculated using reaction rates of chemical reactions and acid-base equilibrium in water. The calculated concentrations and pH values are in good agreement with measured data within the range where the significant changes of the measured data are observed. The rate constant for ONOOH generation is estimated to be 7.8×10^3 $M^{-2}\cdot s^{-1}$, and this value is in good agreement with previously reported values. The generation rates of H_2O_2, NO_2^-, and NO_3^- are estimated to be 7.70×10^{-7}, 4.10×10^{-7}, and 1.10×10^{-7} $M\cdot s^{-1}$, respectively.

1. Introduction

Discharge plasma in contact with water and in water vapor has been recently applied to a wide range of applications, such as biomolecule decontamination[1)], nanoparticle synthesis[2)], plant growth promoting[3)], the degradation of organic compounds[4,5)], disinfection[6-15)], and the treatment of cancer cells.[16,17)] In general, active species, such as electrons, ions, radicals, and reactive neutral species, are generated in plasma, and these species dissolve in water when the plasma is generated in contact with the water. Then, reactive oxygen species (ROS), such as H_2O_2 and HO_2, are generated in the water, and reactive nitrogen species (RNS), such as HNO_2 and ONOOH, are also generated when nitrogen gas is contained in the ambient and/or dissolved gases. The water containing ROS/RNS is well known as plasma-treated water[8-12)], which is also called plasma-activated water[13-15)] and plasma-activated medium.[16,17)] Since ROS/RNS have high oxidation potential, these potentially contribute to bactericidal applications, and the bactericidal mechanisms induced by ROS/RNS in plasma-treated water has been partially elucidated. Ikawa *et al.*[11)] exposed distilled water to low-temperature atmospheric pressure helium plasma, demonstrated the bactericidal activity of ROS/RNS in the water by mixing with *Escherichia coli* suspension, and reported that the bactericidal activity is enhanced under acidic conditions. It was suggested that HO_2 released from O_2NOOH plays an important role in imparting the bactericidal activity to the water. It was also suggested that O_2NOOH is generated by the reaction between ONOOH and H_2O_2, and that ONOOH is generated from HNO_2 and H_2O_2. Some of these species are in equilibrium with those conjugate base in water; therefore, the pH value of the water significantly affect the concentrations of acid and its conjugated base.

Several groups reported ROS/RNS concentrations in water exposed to plasma with the biocidal effects and oxidative strength of those species. Gils *et al.*[12)] produced plasma-treated water using an atmospheric pressure argon plasma jet for inactivation of *Pseudomonas aeruginosa*, and reported the significant influence of the acidity of the plasma-treated water on bactericidal effect. They also calculated ROS/RNS concentrations in the liquid phase using zero-dimensional solution kinetics simulations, estimated the flux of O_3, NO, and OH, and compared the calculated concentrations of H_2O_2, NO_2^-, and NO_3^- with those measured concentrations; however, the chemical equilibrium of species and the reactions of long-lived species (*e.g.* the reaction between HNO_2 and H_2O_2) are not considered. Lukes *et al.*[13)] reported the concentrations of H_2O_2, NO_2^-, and NO_3^- in plasma-exposed water as functions of treatment time and post-discharge time, and that the bactericidal effects of the water is enhanced under acidic conditions. They also reported the rate constant for ONOOH

generation, estimated by a kinetic study of post-discharge processes in pH-buffered aqueous solution. Anderson *et al.*[5] exposed a pH-buffered aqueous solution containing indigo carmine to non-equilibrium atmospheric-pressure plasma, and estimated the branching ratios of OH/NO_2 and NO_3^-/H^+ generation through ONOOH decomposition. Hence, the bactericidal effects and oxidative strength of ROS/RNS and the reactions of ROS/RNS have been well investigated; however, ROS/RNS concentration variations in plasma-exposed water accompanied with the pH variation of the water, caused by dissolving ROS/RNS in the water, have not yet been fully reproduced by solution kinetics simulation, and it contributes to predicting the reactions of ROS/RNS and estimating the generation rate of ROS/RNS in the liquid phase.

In this work, the variations of ROS/RNS concentrations and pH value in water exposed to plasma were calculated by using reaction rates based on acid-base equilibrium and chemical reactions. Our previous work[18] suggested that various discharge plasmas above water, which are a pulsed discharge, a DC corona discharge, and a plasma jet, generate H_2O_2, NO_2^-, and NO_3^- in the water, and discussed the generation process of those species in the gas and liquid phase; however, measurement conditions in the previous work, such as post-discharge time to start analysing plasma-exposed water, were not necessarily the same. Thus, the ROS/RNS concentrations and pH value in water exposed to the pulsed-discharge plasma, which is effective in ROS/RNS generation using the plasmas, were remeasured under the unified conditions in this work. Then, the variations of ROS/RNS concentrations and pH value in the water were calculated by using reaction rates of chemical reactions in water.

2. Experimental apparatus and conditions

The pulsed discharge was generated in the same manner as in our previous work.[18] A cylindrical discharge chamber to generate the pulsed discharge consisted of a needle electrode and a water bath electrode. The needle electrode was a stainless-steel needle with 4.0 mm in diameter and 35 mm in length, and the water bath electrode was made of stainless steel with 119 mm in inner diameter, 12 mm in depth, and a capacity of 0.13 L. Deionized water of 100 mL was poured into the water bath electrode, and the distance between the tip of the needle electrode and the water surface was fixed at 4 mm. Nitrogen gas was fed into the chamber at a constant flow rate of 5 $L \cdot min^{-1}$. A pulsed high voltage with a pulse width of 500 ns generated by a Blumlein generator, which has two coaxial transmission lines, was applied to the needle electrode to generate the pulsed discharge above the water surface. The coaxial transmission lines were charged to a negative voltage of 14.14 kV, and a pulse

repetition rate was 20 pulses per second. The pH value of the water and the ROS/RNS concentrations in the water were measured 4 min after plasma exposure. The pH value and temperature of the water and the ROS/RNS concentrations in the water were measured 4 min after plasma exposure. The pH value and temperature were measured using a pH meter (CyberScan PCWP10), and 1.2 mL of water sample, taken from the plasma-exposed water, were analyzed using a high-performance liquid chromatograph (HPLC; Shimadzu Prominence) equipped with an ion chromatography column (Shodex IC NI-424) in combination with an absorbance detector. The wavelength of the absorbance detector was fixed at 220 nm. The eluent of the HPLC was a mixed aqueous solution of 3 mM ($mmol \cdot L^{-1}$) acetic acid and 1.9 mM potassium hydroxide, the pH value of the solution was 5.1, and the column bath temperature of the HPLC was set to 40°C.

3. Results and discussion

Figures 1(a), 1(b), and 1(c) show photographs of the pulsed-discharge plasma immediately, 5 min, and 30 min after plasma exposure, respectively. The discharge reaches the water surface, and then splits into several branches. A single thick discharge reaches the rim of the water bath electrode immediately after plasma exposure, and several thin discharges that do not reach the rim of the water bath electrode spread over the water surface after 5 min of the plasma exposure. The extension of the discharge along the water surface tends to decrease; the discharge area is about 100 mm in diameter after 5 min of plasma exposure, and about 60 mm in diameter after 30 min of plasma exposure. Figure 2 shows the variations of water temperature as a function of the exposure time. The water temperature shows a tendency to increase and then become constant with the plasma exposure.

Figure 3 shows the chromatogram of the sample after 20 min of plasma exposure. H_2O_2, NO_2^-, and NO_3^- were detected at the retention time of 1.7, 11.6, and 18.0 min, respectively. According to Refs. 11-13, ONOOH and O_2NOOH, which are key species in bactericidal applications, can be produced in plasma-exposed water; however, the peaks corresponding to those species were not detected as shown in Fig. 3. This is due to the lifetime of those species. Since the half-life of ONOOH is typically less than 1 s, ONOOH is decomposed to long-lived species, such as NO_3^-. The lifetime of O_2NOOH depends on temperature[19] and pH[20], becoming shorter at higher temperature and higher pH. Nakashima *et al.*[21] reported that O_2NOOH was detected at a column bath temperature of below 25°C but not at that of 40°C using an eluent of pH 2 in ion-exchange chromatography, because O_2NOOH decomposed to nitrous acid and nitrate between the injector and detector. In this work, the

column bath temperature and the pH value of eluent were set to 40°C and 5.1, respectively; therefore, O_2NOOH in water is completely decomposed between the injector and detector, and this results in no peak of O_2NOOH. Figure 4 shows the concentrations of H_2O_2, NO_2^-, and NO_3^- in the sampled water and the pH value of the water as functions of the exposure time. H_2O_2 and NO_3^- concentrations increase monotonously with the exposure time, while NO_2^- concentration increases, reaches its peak, and then decreases to zero. This result shows a similar tendency, obserbed in the previous work[18], and these species were generated by dissolving H_2O_2, HNO_2, and HNO_3 in water.[13,22-29] Therefore, chemical reactions shown in Table I are deduced. Since the pH value decreases with the increase of the exposure time, the concentration of HNO_2, which is in equilibrium with NO_2^- ($pK_a = 3.3$)[13], increases and reacts with H_2O_2 to form ONOOH. Therefore, NO_2^- concentration drops off in the presence of H_2O_2 and the decrease of pH value. Furthermore, ONOOH is an unstable species and changes into NO_2/OH or NO_3^-/H^+. OH and NO_2 may change into H_2O_2 and NO_2^-/NO_3^- via the reactions shown by the reactions shown by Eqs. (3) and (4), respectively.

According to the chemical reactions in water shown in Table I, the concentration variations of ROS/RNS in water exposed to pulsed-discharge plasma were calculated by using the reaction rates of the reactions. Since H_2O_2, NO_2^-, and NO_3^- were generated as ROS/RNS in water by the plasma exposure, it was assumed that H_2O_2, NO_2^-, and NO_3^- were generated in water with the plasma exposure. Accordingly, the reaction rates are represented as follows:

$$[NO_2^-] = f([NO_2^-] + [HNO_2]), \quad (5)$$

$$[HNO_2] = (1 - f)([NO_2^-] + [HNO_2]), \quad (6)$$

$$\frac{d[ONOOH]}{dt} = k_1[H_2O_2][HNO_2][H^+] - k_2[ONOOH], \quad (7)$$

$$\frac{d[HNO_2]}{dt} = -k_1[H_2O_2][HNO_2][H^+], \quad (8)$$

$$\frac{d[H_2O_2]}{dt} = G_{H_2O_2} - k_1[H_2O_2][HNO_2][H^+] + k_3[OH], \quad (9)$$

$$\frac{d[NO_2^-]}{dt} = G_{NO_2^-} + k_4[NO_2], \quad (10)$$

$$\frac{d[NO_3^-]}{dt} = G_{NO_3^-} + 0.76k_2[ONOOH] + k_4[NO_2], \quad (11)$$

$$\frac{d[OH]}{dt} = 0.24k_2[ONOOH] - 2k_3[OH]^2, \quad (12)$$

$$\frac{\mathrm{d}[\mathrm{NO_2}]}{\mathrm{d}t} = 0.24k_2[\mathrm{ONOOH}] - 2k_4[\mathrm{NO_2}]^2, \qquad (13)$$

where [X] is the concentration of the species X at time t, f is the ionization degree of HNO_2, G_X is the generation rate of the species X, and k_1, k_2, k_3, and k_4 are the rate constants for the reactions shown by Eqs. (1), (2), (3), and (4), respectively. The coefficients 0.76 and 0.24 in Eqs. (11)-(13) are originated in the branching ratios of the reaction shown by Eq. (2). The value of f is determined by pK_a for HNO_2 and the pH value of the water. The values of the rate constants k_2, k_3, and k_4 were reported as $0.13 + 0.87[H^+]$ s^{-1} in Ref. 5, 4.2×10^9 $M^{-1}\cdot s^{-1}$ in Ref. 31, and 1.0×10^8 $M^{-1}\cdot s^{-1}$ in Ref. 32, respectively. The concentrations of H_2O_2, NO_2^-, NO_3^-, HNO_2, ONOOH, OH, and NO_2 and the pH value in the water, determined by NO_2^- and NO_3^- concentrations, were calculated by using the above reaction rates, and those were fitted to the measured data, as shown in Fig. 2, by varying the rate constant k_1 and the generation rates of H_2O_2, NO_2^-, and NO_3^-. The concentration distribution was assumed to be uniform, and the time variation of concentrations during post-discharge period to start analyzing the plasma-exposed water and the pH variation in the liquid chromatographic analysis were considered. The above equations were calculated by the Runge-Kutta fourth-order method.

Figure 5 shows the calculated concentrations of ROS/RNS and pH value, together with the measured data as functions of time. The calculated concentrations of H_2O_2, NO_2^-, and NO_3^- and pH value were in approximate agreement with the measured data below 3000 s, when k_1 was estimated to be 7.8×10^3 $M^{-2}\cdot s^{-1}$ and the generation rates of H_2O_2, NO_2^-, and NO_3^- were estimated to be 7.70×10^{-7}, 4.10×10^{-7}, and 1.10×10^{-7} $M\cdot s^{-1}$, respectively. The estimated value of the rate constant k_1 is in good agreement with previously reported values, $8.3(\pm0.6)\times10^3$ $M^{-2}\cdot s^{-1}$ in Ref. 33, 4.6×10^3 ($\pm$ 20%) $M^{-2}\cdot s^{-1}$ in Ref. 34, and $(6.3\pm1.5)\times10^3$ $M^{-2}\cdot s^{-1}$ in Ref. 35. The calculated concentrations and pH were overestimated comparing to the measured data above 3000 s. This may be due to the change of the generation rate. Although the generation rates of H_2O_2, HNO_2, and HNO_3 were assumed to be constant in the calculation, the generation rates may decrease since the discharge area was contracted with time as shown in Fig. 1. The water temperature affects the reaction constant of chemical reactions in water, and the temperature change was observed as shown in Fig. 2. The calculated concentrations of ROS/RNS were in good agreement with measured data within the range where the temperature change was observed; therefore, the ROS/RNS generation rates may be significantly affected not by the temperature change but by the contraction of the discharge area.

This work suggests that the simple model considering only four reactions shown in Eqs.

(1)-(4) with the assumption of complete mixing in the liquid phase can roughly reproduce the measured data, so that it may allow to roughly estimate the generation rates of H_2O_2, NO_2^-, and NO_3^- and evaluate the generation efficiencies of those species. In order to simulate the generation of ROS/RNS in liquid more accurately, it is desirable to consider the variations of the generation rate depending on the discharge area and the temperature dependence of the rate constants of chemical reactions in water.

4. Conclusions

The concentrations of ROS/RNS and pH value in pulsed-discharge exposed water were remeasured under the unified conditions and calculated using reaction rates based on acid-base equilibrium and chemical reactions in the water. H_2O_2, NO_2^-, and NO_3^- were generated as a similar tendency in our previous work. The calculated concentrations of H_2O_2, NO_2^-, and NO_3^- and pH value in the water exposed to the pulsed-discharge plasma were in approximate agreement with the measured data below 3000 s, when the rate constant for ONOOH generation was set to 7.8×10^3 $M^{-2}\cdot s^{-1}$, which is in good agreement with previously reported values. The generation rates of H_2O_2, NO_2^-, and NO_3^- were estimated to be 7.70×10^{-7}, 4.10×10^{-7}, and 1.10×10^{-7} $M\cdot s^{-1}$, respectively.

Acknowledgments

This work was partly supported by JSPS KAKENHI Grant Number JP17J11124.

References

1) F. Fumagalli, O. Kylián, L. Amato, J. Hanus, and F. Rossi, J. Phys. D **45**, 135203 (2012).
2) N. Shirai, S. Uchida, and F. Tochikubo, Jpn. J. Appl. Phys. **53**, 046202 (2014).
3) D. P. Park, K. Davis, S. Gilani, C.-A. Alonzo, D. Dobrynin, G. Friedman, A. Fridman, A. Rabinovich, and G. Fridman, Curr. Appl. Phys. **13**, S19 (2013).
4) G. Tang, A. Komuro, K. Takahashi, and A. Ando, J. Plasma Fusion Res. **11**, 2406025 (2016).
5) C. E. Anderson, N. R. Cha, A. D. Lindsay, D. S. Clark, and D. B. Graves, Plasma Chem. Plasma Process. **36**, 1393 (2016).
6) D. Dobrynin, G. Friedman, A. Fridman, and A. Starikovskiy, New J. Phys. **13**, 103033 (2011).
7) Q. Zhang, P. Sun, H. Feng, R. Wang, Y. Liang, W. Zhu, K. H. Becker, J. Zhang, and J. Fang, J. Appl. Phys. **111**, 123305 (2012).
8) A. Kojtari, U. K. Ercan, J. Smith, G. Friedman, R. B. Sensenig, S. Tyagi, S. G. Joshi, H.-F. Ji, and A. D. Brooks, J. Nanomedicine Biother. Discov. **4**, 1000120 (2013).
9) H.-S. Kim, K. C. Wright, I.-W. Hwang, D.-H. Lee, A. Rabinovich, A. Fridman, and Y. I. Cho, Int. Commun. Heat Mass Transf. **42**, 5 (2013).
10) M. Naïtali, G. Kamgang-Youbi, J.-M. Herry, M.-N. Bellon-Fontaine, and J.-L. Brisset, Appl. Environ. Microbiol. **76**, 7662 (2010).
11) S. Ikawa, A. Tani, Y. Nakashima, and K. Kitano, J. Phys. D. **49**, 425401 (2016).
12) C. A. J. van Gils, S. Hofmann, B. K. H. L. Boekema, R. Brandenburg, and P. J. Bruggeman, J. Phys. D **46**, 175203 (2013).
13) P. Lukes, E. Dolezalova, I. Sisrova, and M. Clupek, Plasma Sources Sci. Technol. **23**, 015019 (2014).
14) M. J. Traylor, M. J. Pavlovich, S. Karim, P. Hait, Y. Sakiyama, D. S. Clark, and D. B. Graves, J. Phys. D. **44**, 472001 (2011).
15) Q. Zhang, Y. Liang, H. Feng, R. Ma, Y. Tian, J. Zhang, and J. Fang, Appl. Phys. Lett. **102**, 203701 (2013).
16) S. Mohades, M. Laroussi, J. Sears, N. Barekzi, and H. Razavi, Phys. Plasmas **22**, 122001 (2015).
17) J. Ikeda, H. Tanaka, K. Ishikawa, H. Sakakita, Y. Ikehara, and M. Hori, Pathol. Int. **68**, 23 (2018).
18) K. Takahashi, K. Satoh, H. Itoh, H. Kawaguchi, I. Timoshkin, M. Given, and S. MacGregor, Jpn. J. Appl. Phys. **55**, 07LF01 (2016).

19) J.-M. Régimbal and M. Mozurkewich, J. Phys. Chem. A, **101**, 8822 (1997).
20) R. A. Kenley, P. L. Trevor, and B. Y. Lan, J. Am. Chem. Soc. **103**, 2203 (1981).
21) Y. Nakashima, S. Ikawa, A. Tani, and K. Kitano, J. Chromatogr. A. **1431**, 89 (2016).
22) Y. Itikawa and N. Mason, J. Phys. Chem. Ref. Data **34**, 1 (2005).
23) W. Lindinger, Phys. Rev. A **7**, 328 (1973).
24) R. P. Joshi and S. M. Thagard, Plasma Chem. Plasma Process. **33**, 17 (2013).
25) R. Atkinson, D. L. Baulch, R. A. Cox, J. N. Crowley, R. F. Hampson, R. G. Hynes, M. E. Jenkin, M. J. Rossi, and J. Troe, Atmos. Chem. Phys. **4**, 1461 (2004).
26) S. Mededovic and B.R. Locke, J. Phys. D **40**, 7734 (2007).
27) R. Atkinson, D. L. Baulch, R. A. Cox, R. F. Hampson, Jr., J. A. Kerr, and J. Troe, J. Phys. Chem. Ref. Data **18**, 881 (1989).
28) S. Goldstein, J. Lind, and G. Marényi, Chem. Rev. **105**, 2457 (2005).
29) L. D'Ottone, P. Campuzano-Jost, D. Bauer, and A. J. Hynes, J. Phys. Chem. A **105**, 10538 (2001).
30) G. Merényi, J. Lind, G. Czapski, and S. Goldstein, Inorg. Chem. **42**, 3796 (2003).
31) A. J. Elliot and D. R. McCracken, J. Chem. Soc. Faraday Trans. **86**, 1539 (1990).
32) Y.-N. Lee and S. E. Schwartz, J. Phys. Chem. **85**, 840 (1981).
33) E. Halfpenny and P. L. Robinson, J. Chem. Soc. 928 (1952).
34) D. E. Damschen and L. R. Martin, Atmos. Environ. **17**, 2005 (1983).
35) Y.-N. Lee and J. A. Lind, J. Geophys. Res. Atmos. **91**, 2793 (1986).

Figure Captions

Fig. 1. (Color online) Photographs of pulsed-discharge plasma: (a) Immediately after plasma exposure, (b) After 5 min of plasma exposure, and (c) After 30 min of plasma exposure.

Fig. 2. (Black and white) The variations of water temperature.

Fig. 3. (Color online) Chromatogram of a sample taken after 20 min of plasma exposure.

Fig. 4. (Color online) The variations of concentrations and pH value as functions of exposure time: (a) concentrations and (b) pH.

Fig. 5. (Color online) Comparison of calculated and measured concentrations and pH value: (a) H_2O_2, (b) NO_2^-, (c) NO_3^-, and (d) pH.

Table I. ROS/RNS reactions in water.

Reaction	Eq.	Ref.
$HNO_2 + H_2O_2 + H^+ \rightarrow ONOOH + H_2O + H^+$	(1)	27)
$ONOOH \rightarrow NO_2 + OH$ (24%) or $NO_3^- + H^+$ (76%)	(2)	13)
$OH + OH \rightarrow H_2O_2$	(3)	28)
$2NO_2 + H_2O \rightarrow NO_2^- + NO_3^- + 2H^+$	(4)	29)

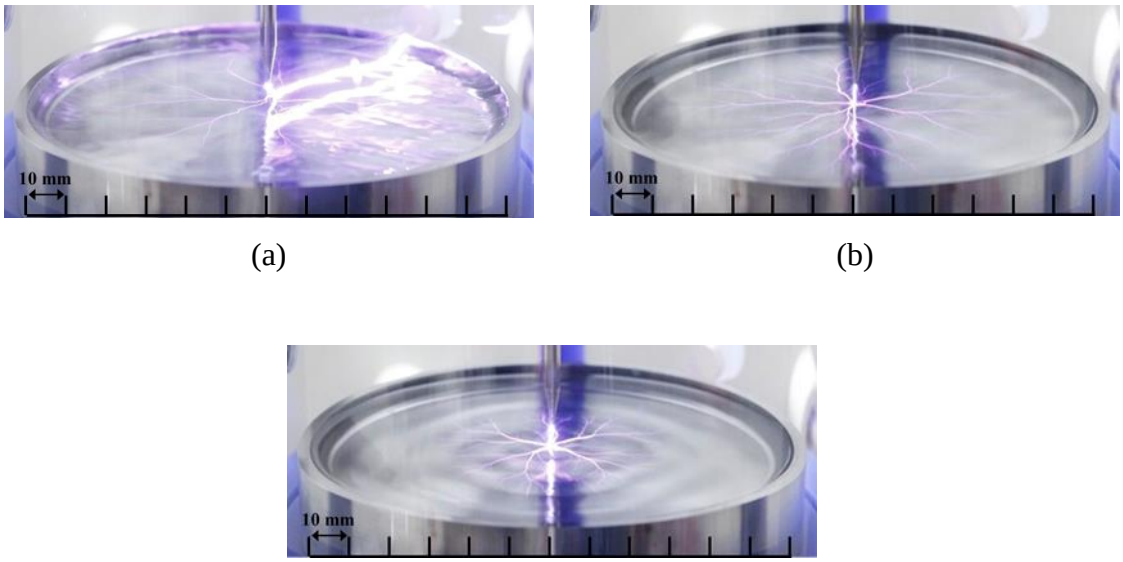

(a) (b)

(c)

Fig. 1. (Color Online)

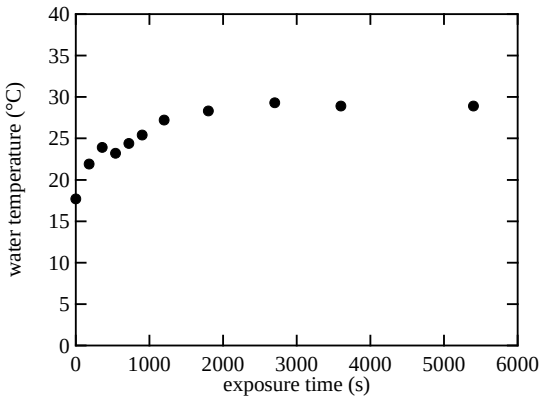

Fig. 2. (Black and white)

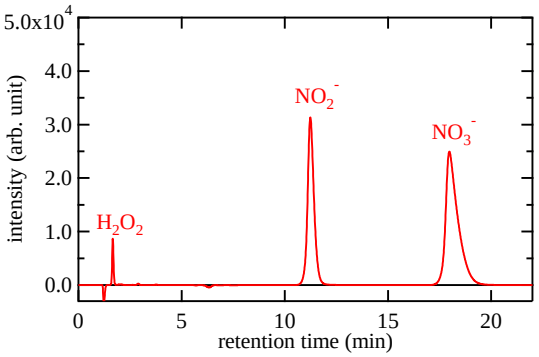

Fig. 3. (Color Online)

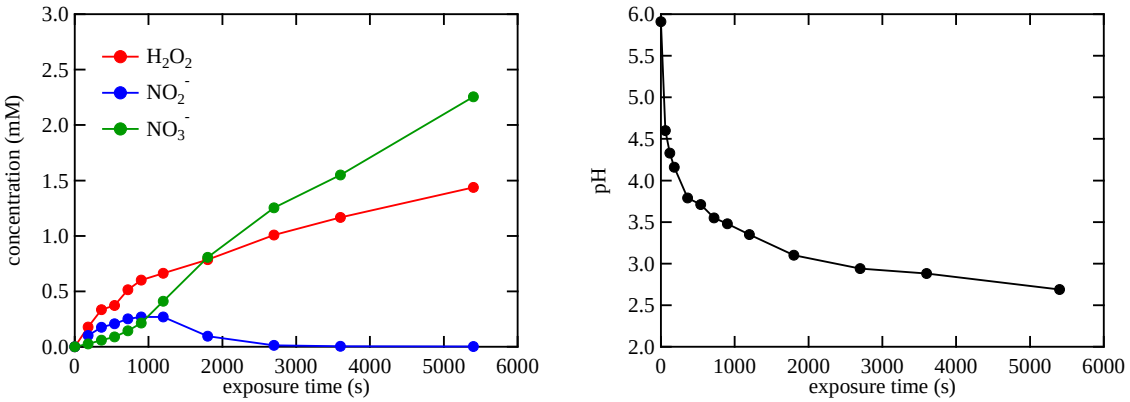

(a) (b)

Fig. 4. (Color Online)

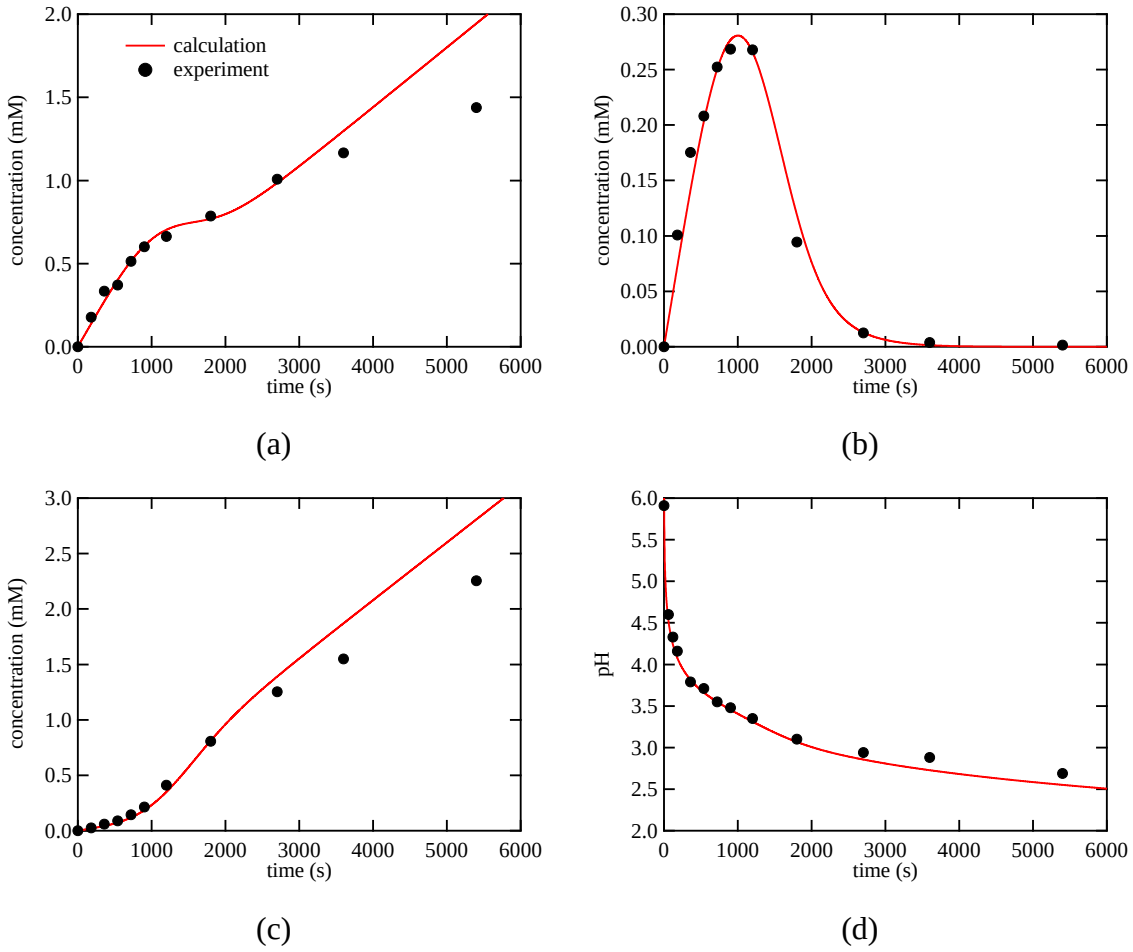

Fig. 5. (Color Online)